DOI 10.5012/bkcs.2011.32.8.2571

Study on the Dominant Film-Forming Site Among Components of $Li(Ni_{1/3}Co_{1/3}Mn_{1/3})O_2$ Cathode in Li-ion Batteries

Ketack Kim,[*] Daewoong Kam,[†] Cao Cuong Nguyen,[‡] Seung-Wan Song,[‡] and Robert Kostecki[§]

Department of Chemistry, Sangmyung University, Seoul 110-743, Korea. [*]E-mail: ketack.kim@smu.ac.kr
[†]Battery Research Center, Korea Electrotechnology Research Institute, Changwon 641-600, Korea
[‡]Department of Fine Chemical Engineering & Applied Chemistry, Chungnam National University, Daejeon 305-764, Korea
[§]Environmental Energy Technologies Division, Lawrence Berkeley National Laboratory, Berkeley, CA 94720, USA
Received April 20, 2011, Accepted June 17, 2011

Surface film formation on $Li(Ni_{1/3}Co_{1/3}Mn_{1/3})O_2$ cathodes upon oxidation of electrolyte during electrochemical cycling was investigated. Information on the important factors for film formation on the cathode can facilitate the design of additives that improve the properties of the cathode. Pyrazole is added to the electrolyte because it is readily oxidized to form a surface film on the cathode. The results of differential scanning calorimetry and Fourier transform infrared spectroscopy (FTIR) showed that the active material played a dominant role in the interfacial film formation with the electrolyte. Carbon black played a negligible role in the surface film formation.

Key Words : Li-ion battery, $Li(Ni_{1/3}Co_{1/3}Mn_{1/3})O_2$ cathode, Electrolyte decomposition

Introduction

The development of plug-in hybrid electric vehicles (PHEVs) and large stationary energy storage devices requires high-energy-density Li-ion batteries with high-voltage cathode active materials. However, high-voltage cathode materials (e.g., $Li(Ni_{1/3}Mn_{1/3}Co_{1/3})O_2$, (NMC)) are frequently exposed to voltages above 4.2 V *vs*. Li/Li^+. At such voltages, the electrolyte tends to oxidize on the surface of the cathode. To prevent continuous oxidation of the electrolyte, leading to its decomposition, and to improve the safety and cycling performance of Li-ion batteries, electrolyte additives are often used to stabilize the cathode/electrolyte interface.[1-3] The effects of flame retardant additives,[4] thermal protection films,[5] and solid-electrolyte-interphase (SEI) formation due to oxidative electrolyte decomposition[6] on the electrochemical behavior of Li-ion cathodes have been studied and reported.[4,7-9]

A basic understanding of the interfacial processes of composite cathodes in Li-ion batteries is essential for improving battery electrochemical performance and safety. The rational design and selection of electrolyte additives with specific functional groups determines the electrocatalytic activity of cathodes and influences the surface reaction mechanism. Pyrazole additive is an interesting candidate to help stabilize the NMC cathode/electrolyte interface because it effectively oxidizes at approximately 3.5 V *vs*. Li/Li^+ and forms a thick, dense film on the surface of the cathode.[10] Pyrazole oxidation products tend to catalyze the subsequent electrolyte oxidation and formation of an overlying surface film during the operation of lithium cells.[10] Using pyrazole as an additive to the electrolyte can be useful for observing surface films on the cathode because of its oxidative properties.

A typical composite cathode usually consists of an active cathode material, a carbon black conductive additive, and a polymeric binder. Although the typical weight ratio between carbon additives and the cathode active material does not exceed ~0.15, the surface area ratio can range from ~0.5 to 200, depending on the morphology and topology of carbon additives and the active material. Surface reactions that can disturb the distribution of the conductive additive or change the electronic properties of the conductive carbon matrix can degrade the electrochemical performance of the composite cathode.[11] However, thus far, there have been no detailed studies on the mechanisms of the surface reactions at individual electrode components. In fact, the electrocatalytic activity of the active cathode material *vs*. the carbon additive and the possible interference between surface reactions remain unexplored.

In this work, we report on interfacial reactions of the NMC composite cathode in the organic carbonate electrolyte. The relative reactivity of the $Li(Ni_{1/3}Mn_{1/3}Co_{1/3})O_2$ and the carbon black additive in the composite cathode toward the oxidation of the electrolyte was systematically studied and compared. We sensed and probed the surface film formation using differential scanning calorimetry (DSC) and attenuated total reflectance Fourier transform infrared (ATR-FTIR) spectroscopy. DSC provided direct insight into the thermal stability of the NMC cathode and correlation with the effect of the stable surface film.[10] IR spectroscopy offered direct information on the composition and structure of the surface species produced at the NMC cathode surface.

Experimental

$Li(Ni_{1/3}Mn_{1/3}Co_{1/3})O_2$ (Daejung Chemical & Metal), poly(vinylidene fluoride) (PVdF, Aldrich), 1.0 M $LiPF_6$ in ethylene carbonate/diethyl carbonate (EC/DEC, 1:1 vol.) (Techno

Semichem), dimethyl carbonate (DMC, Techno Semichem), and pyrazole (Aldrich) were used as purchased. The NMC was well mixed with carbon black (Super-P Black, Timcal Carbon), and PVdF in *N*-methyl-2-pyrrolidone (NMP, Junsei) was used to prepare the mixed slurry for the cathode fabrication. The slurry was coated onto an Al foil and dried overnight at 120 °C, followed by hot roll pressing to reduce the thickness by 20%. To investigate the surface film formation processes on the individual cathode components, three different electrodes were prepared: electrode A, a composite cathode with all components (NMC:carbon black:PVdF, 86:8:6); electrode B, a composite electrode with no carbon additive; and electrode C, an electrode with no NMC active material. The electrode component ratios are presented in Table 1. The cathodes for DSC tests were prepared in 2032-type coin cells (Hohsen Corp.) with Li-foil as an anode. A 15-mm-thick separator (Celgard 2500) was placed between the cathode and the anode. The electrolyte (with or without 3 wt % pyrazole additive) was used in coin cells. The entire cell preparation process was conducted in a dry room with the moisture content maintained below 10 ppm. To study surface film formation, the coin cells were charged and discharged 10 times, i.e., cycled between 2.8 V and 4.3 V at a rate of C/2 (1 C rate = 170 mA/g of the NMC) using a galvanostatic cycler (TOSCAT-2100U, Toyo Systems Co.). This cycling process was stopped when the coin cells were in a charged state at 4.3 V for DSC tests and IR measurements. The thermal stability of the cathodes and the film formation on the cathode surface after cycling was investigated using DSC (Q1000, TA). Excess solvent was removed from the cathode by spontaneous evaporation in the dry room for 3-hrs. Complete removal of the solvent using vacuum was not required because the thickness of the surface film and the charged level of the cathode for the DSC measurements could be changed by controlling the drying conditions. DSC scans were carried out with the charged cathode at a heating rate of 5 °C/min from 40 to 400 °C under a nitrogen atmosphere. Cyclic voltammetry (CV) measurements in a coin-type three-electrode cell (Hohsen Corp.) were conducted using a potentiostat (VSP3, Princeton Applied Research). Electrode A was used for the CV cycles. Two pieces of lithium foil were placed near the cathode as a counter and a reference electrode. The potential was initially set to the open circuit potential (~3.4 V) and then scanned between 2.8 and 4.3 V *vs*. Li/Li^+ at a scan rate of 0.2 mV/ s.

The surface of the cycled electrodes (unwashed and washed with DMC) was examined with *ex situ* ATR-FTIR spectroscopy using an IR spectrometer equipped with a mercury-cadmium-telluride detector. The cycled cathodes were removed from the coin cells and dried at room temperature in an Ar-filled glove box so as to not damage the functional groups containing oxygen. Prior to the FTIR measurements, the cathodes were directly mounted on the enclosed single-reflection ATR Ge crystal in the Ar-filled glove box. The cathodes were never exposed to the air during transportation of the sample from the glove box to the IR instrument or during FTIR measurement. The spectral resolution was 4 cm^{-1}, and a total of 512 scans were accumulated. The spectra were corrected for the light penetration depth as a function of wavelength. To examine the IR contribution from the electrolyte residue, a reference sample made of stainless steel (SS) was prepared. This sample was immersed in the electrolyte for 24 hrs and was subsequently dried at room temperature in the glove box.

Table 1. Composition of the three electrodes prepared for DSC and IR spectroscopic investigation

Electrode	NMC:carbon black:PVdF ratio
A	86:8:6
B	80:0:20
C	0:80:20

Results and Discussion

Electrochemical Measurements. Figure 1 shows cyclic voltammograms for the NMC cathode with and without the pyrazole additive. The cathode without the additive (Fig. 1(a)) exhibited several anodic and cathodic peaks, which correspond to lithium intercalation/deintercalation at 4.14 V and 3.45 V at the tenth cycle, respectively. The unstable current in the first cycle represents the electrolysis of the electrolyte and a wetting process of the cathode by the electrolyte. The current peaks experienced only small changes in position and intensity during the following scans. However, CV of the NMC cathode with the pyrazole additive (Fig. 1(b)) displayed a relatively wide cathodic and anodic peak separation during the first two cycles. Moreover, three new anodic peaks, denoted as α, δ, and γ (at 4.24, 4.04, and 3.90 V, respectively), appeared on the CV. With increasing cycle number, the α and α' peaks gradually shifted closer to each other and eventually overlapped with the β and β' peaks, which were similar to the CV peaks observed at 4.14 and 3.45 V during the tenth cycle for the NMC cathode without the additive. The wide peak separation and new peaks all originated from the addition of pyrazole. Nevertheless, the peaks γ, δ, and γ' rapidly diminished following the second cycle.

To study the behavior of the three anodic peaks of α, γ, and δ, CVs were recorded within different anodic scan limits, i.e., 4.0, 4.1, and 4.3 V (Fig. 1(c)). The cathodic peak in the first (2.5-4.0 V) and second (2.5-4.1 V) cycles shifted from 3.51 to 3.46 V, respectively, which implies that the peaks γ, δ, and γ' were not related to the redox peaks of NMC, i.e., α and α' could be assigned to the electrochemical surface reactions with pyrazole. The third cycle to 4.3 V showed the primarily redox current response of the NMC near 4.22 and 3.35 V, but the reduction current of the pyrazole was still clearly visible. The kinetic and/or transport limitations during charging/discharging that resulted from the surface layer formation tended to gradually disappear with cycling, and the CVs tended to resemble those in Figure 1(b).

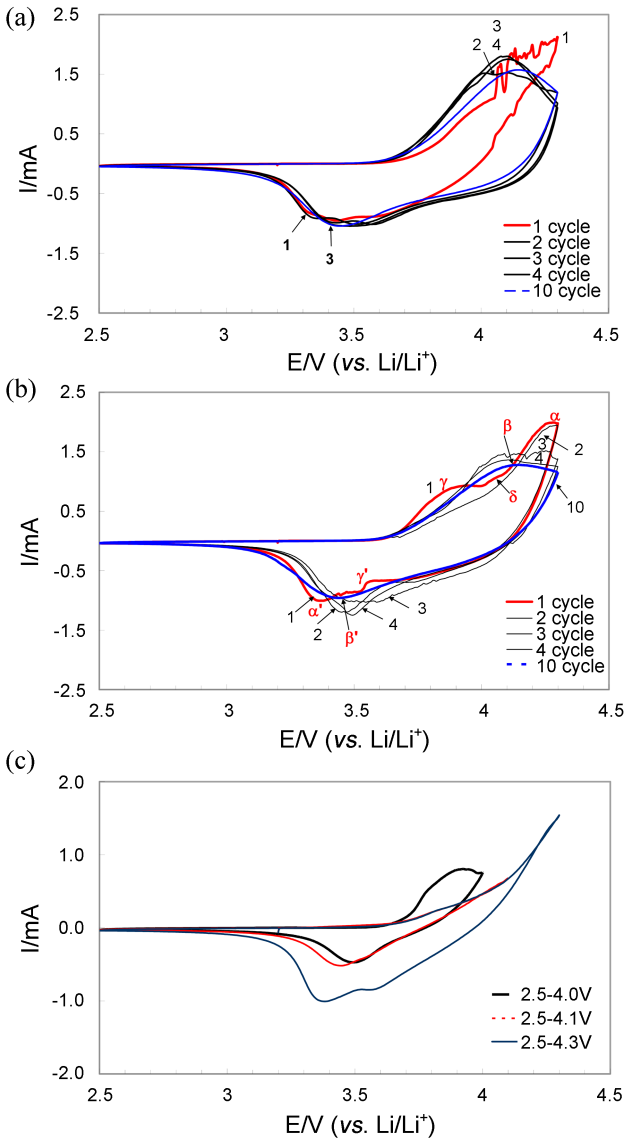

Figure 1. Cyclic voltammograms of the (a) NMC electrode in 1 M $LiPF_6$, EC:DEC (1:1 vol.) without the pyrazole additive, (b) with 3 wt % pyrazole, and (c) with 3 wt % pyrazole at different CV anodic limits.

Examination of the NMC Cathodes Tested using DSC. The effect of pyrazole on the surface film formation and thermal stability of the cathode was examined with DSC. Figure 2 shows a DSC curve for the charged NMC cathode (electrode A) that was cycled at C/2 in 1 M $LiPF_6$, EC:DEC (1:1 vol.) with 3 wt % of the pyrazole additive. A sharp exothermic peak near 110 °C was attributed to the thermal decomposition of the surface film formed on the cathode and is consistent with previous reports.[5,10] A peak at 360 °C corresponds to the oxygen release from the crystal structure of the NMC because of its thermal instability. The oxygen release from NMC usually takes place at 270 °C[5,10,12] in the absence of electrolyte additives. The presence of the surface film of pyrazole decomposition products delayed[10] the exothermic oxygen release[12,13] from the NMC, which indicates that the surface film protects the NMC and enhances the

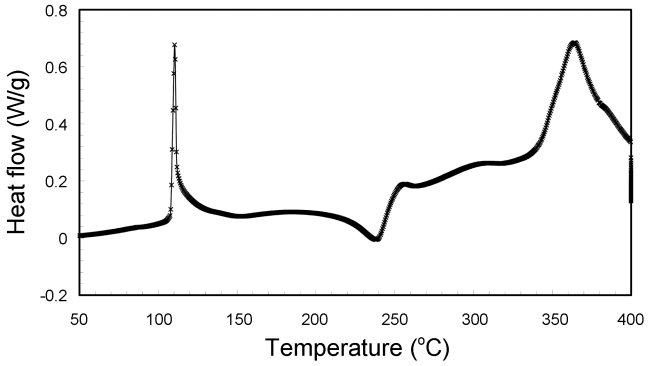

Figure 2. A DSC curve for the NMC electrode A that was cycled 10 times between 2.8 V and 4.3 V at a C/2 rate in 1 M $LiPF_6$, EC:DEC (1:1 vol.) with 3 wt % pyrazole.

thermal stability of the NMC. To understand the effect of the surface film formation on the thermal stability and performance of the cathode, the possible contributions from the individual components in the composite electrode were investigated.

Three different electrodes (Table 1) were prepared; electrode A contained NMC and carbon black, whereas electrodes B and C consisted only of NMC or carbon black, respectively. All electrodes contained the PVdF binder. Electrode B could not be charged completely because of the absence of the conductive carbon black additive. In contrast, electrode C behaved like a double layer capacitor, and no faradaic current was observed. Although electrodes A, B, and C showed radically different current response profiles, 10 repetitive charge/discharge cycles between 2.5 and 4.3 V gave enough charge for film formation and DSC measurements under the given conditions.

Because electrodes B and C had very different elemental ratios than electrode A, they showed no oxygen release peaks in the NMC. We can only discuss the film formation for the electrodes under 200 °C because of the lack of oxygen release reactions. The DSC profiles of electrodes A and B (Fig. 3) show the exothermic peaks due to surface film formation at 110 and 111 °C, respectively. Onset and peak

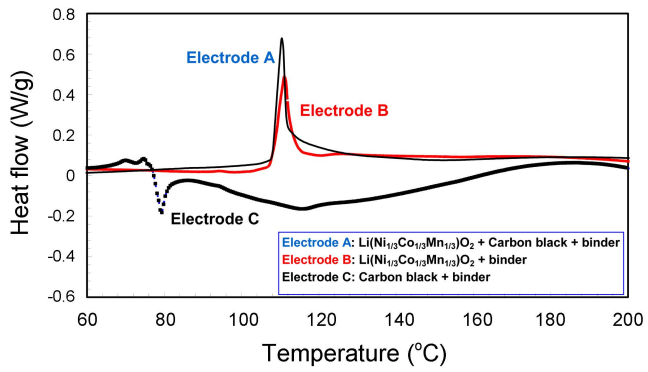

Figure 3. DSC curves for the electrodes A, B, and C after 10 cycles of the cells in 1 M $LiPF_6$, EC:DEC (1:1 vol.) with 3 wt % of pyrazole at a C/2 rate between 2.8 and 4.3 V. The current for electrode C was the same as that applied for electrode A.

temperatures for both electrodes occur at almost identical positions, which indicate that the compositions of the surface films are similar. The larger area of the peak indicated that electrode A accumulated a thicker surface film than electrode B, which only had NMC. It appears that the NMC actively reacts with the electrolyte and forms the surface film. Moreover, carbon black attracts electrolyte adsorbates to the cathode surface and facilitates electrolysis of the electrolyte, and it also provides improved kinetics by supporting the electronic conductivity and particle connection to the NMC, which leads to the formation of a thicker surface film. Electrode C, which included only carbon black, did not show a peak at 110 °C in the DSC data but did show a broad endothermic peak, which is associated with electrolyte evaporation.[14] This result implies that carbon black alone does not result in surface film formation. Carbon black seems to be inactive in the electrolysis of electrolyte components within our operation potential region.

Surface Characterization of Cycled Electrodes using FTIR. The surface film formation on the electrodes was studied using *ex situ* ATR-FTIR spectroscopy. Figure 4(a) shows the IR spectra of the cycled unwashed electrodes, the electrolyte residue on the SS substrate, and a reference spectrum for PVdF. It should be noted that the IR active bands of layered hexagonal structure (*R3-m*) $LiMO_2$-type (e.g., M = Ni, Co) materials were observed below 650 cm^{-1};[15] they are not shown in the spectra. IR bands of lithium carbonate, which has been found to form on the surface of $LiMO_2$-type cathode materials upon exposure to air,[6,16,17] were not observed in the FTIR spectra.

The spectrum of the electrolyte residue (Fig. 4(a)) shows two bands at 1,807 and 1,774 cm^{-1}, characteristic of the EC carbonyl group in the EC:$LiPF_6$ solvate;[18] however, the intensity of the ring-breathing mode at 1807 cm^{-1} was reduced compared with that of solid EC. Other sharp peaks at 903 and 833 cm^{-1} are attributed to the EC ring-bending modes and the P-F stretching from solvated $LiPF_6$.[18] All the bands from the EC:$LiPF_6$ electrolyte residue disappeared after washing with DMC for 10 seconds (not shown).

The FTIR spectra of all unwashed electrodes (Fig. 4(a)-(b)) exhibited prominent peaks at 1,807 and 1,774 cm^{-1} due to the EC:$LiPF_6$ solvate from the electrolyte residue. However, electrode C, which consisted of carbon black, displayed a band at 1,807 cm^{-1} that was relatively stronger than that at 1,774 cm^{-1} when compared with electrodes A and B. Note that solid EC exhibits these two bands at an approximately equal intensity because of the Fermi resonance between the C=O stretching. Thus, the spectral features of sample C appeared to be closer to those of solid EC rather than those of the EC:$LiPF_6$ solvate. The weak spectral response below 900 cm^{-1} and the absence of the P-F stretching band from the EC:$LiPF_6$ solvate supports this assignment. All the FTIR spectra showed a weak contribution from PVdF, with a strong band at 1,400 cm^{-1} from the CH_2 bending mode and two bands at 1,171 and 1,071 cm^{-1} that correspond to ν(C-F).

A close inspection of the spectra in Figure 4(b) clearly

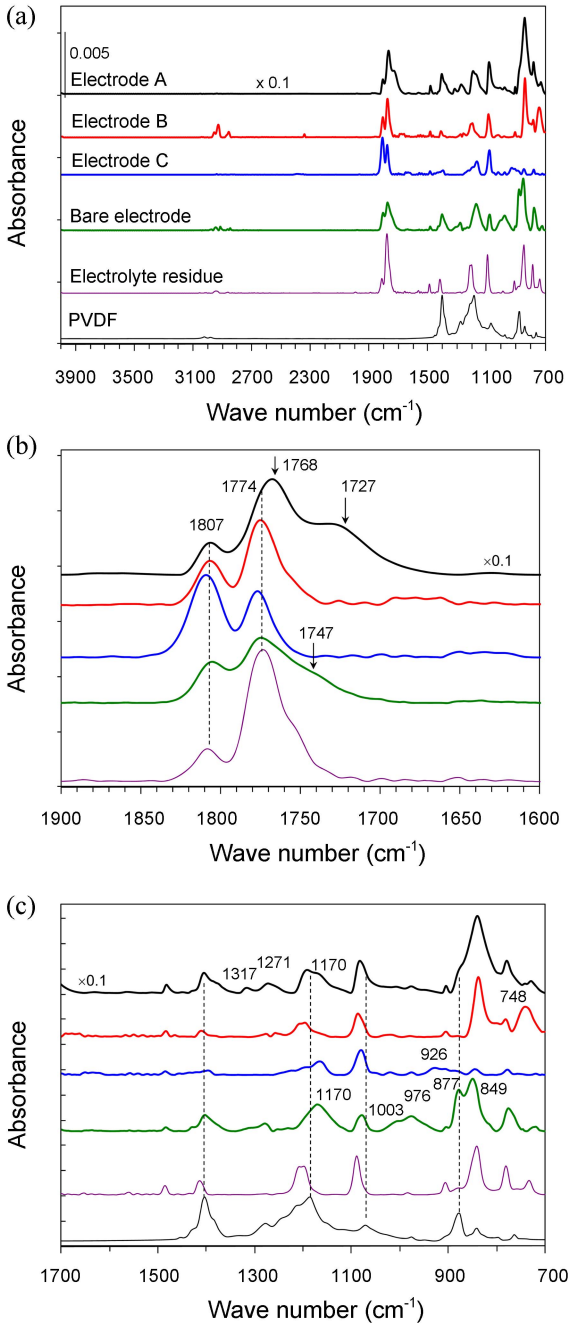

Figure 4. *Ex situ* FTIR spectra of (a) the reference spectrum of PVdF, the stainless steel substrate with electrolyte residue, and the cycled and unwashed bare electrode without the pyrazole additive, along with the cycled and unwashed electrodes A, B, and C after 10 cycles in 1 M $LiPF_6$, EC:DEC (1:1 vol.) with 3 wt % pyrazole at a C/2 rate between 2.8 and 4.3 V, (b) the C=O stretching region of the spectra at 1,900-1,600 cm^{-1}, and (c) the lower wave number region of 1,700-700 cm^{-1}. The current for electrode C was the same as that applied for electrode A.

shows the appearance of new spectral features in the C=O stretching region. The composite electrode "A", which contained both NMC and carbon, exhibited a new feature at 1,768 and 1,727 cm^{-1}, which is attributed to the C=O stretching of the ester groups. The appearance of two other peaks at 1,271 and ~1,090 cm^{-1} (Fig. 4(c)) of nearly equal

intensity confirms the presence of esters[19,20] RCOOR'. The peak at 1,271 cm^{-1} is due to asymmetric C-O-C stretching, and the other one at ~1,090 cm^{-1} corresponds to the asymmetric stretch (O-C-C) mode. The bare cathode, which has the same composition as electrode A but was cycled without pyrazole also showed a broad shoulder near 1,747 cm^{-1}, corresponding to the ester group, together with fingerprints. A significantly larger absorbance for the peaks of electrode A compared with the bare electrode indicates that the concentration level of surface species on the surface of electrode A became much higher than on the bare electrode because of pyrazole and/or the SEI layer thickening.

In situ FTIR data reported in the literature reveals similar functionalities of (poly)ester on $LiCoO_2$ composite cathodes, which originate from the electrochemical oxidation in the "overcharge" potential region of 4.2-4.8 V for propylene carbonate, $LiPF_6$, or $LiBF_4$.[21] In addition, surface species with anhydride and ester functionalities were observed by *ex situ* ATR-FTIR spectroscopy on an $Li(Ni_{0.8}Co_{0.15}Al_{0.05})O_2$ composite cathode upon charging to 4.2 V in 1 M $LiPF_6$, EC:DEC.[6] The proposed mechanism for the film formation involves Li deintercalation and oxygen transfer from the cathode-destabilized oxide lattice to the solvent molecules. It was demonstrated, however, that the structure of the NMC remained stable when charged below 4.4 V (~2/3 Li deintercalation).[22,23] Therefore, we believe that the film formed on the composite electrode A was produced by electron-transfer-induced oxidation of the electrolyte. New features at 1,271 and 1,170 cm^{-1} can be ascribed to P=O stretching[24] of the P=O–containing species and/or the C-O-C asymmetric stretching of the ether group.[19,20] The strong intensity of the peak at 844 cm^{-1} may be associated with the presence of other P-F–containing species in addition to solvated $LiPF_6$. The relevant literature on FTIR studies showed the presence of LiF and $Li_xPF_yO_z$ in the surface film of composite cathodes.[11] Similar surface species were detected by *ex situ* x-ray photoelectron spectroscopy (XPS) on a $LiCoO_2$ cathode cycled in an electrolyte of 1 M $LiPF_6$ in EC and DMC in the voltage region of 3.0-4.7 V,[25] which is consistent with our data. Thus, the electrode surface film seems to include PF-containing species. The major product of $LiPF_6$ decomposition has been known to be LiF,[26] but LiF is invisible in the mid-IR (700-4,000 cm^{-1}) region. Recalling that $LiPF_6$ was in equilibrium with PF_5 and LiF, the PF-containing surface species on the cathode surface might originate from PF_5-derived species, which may indirectly indicate that LiF also forms on the cathode surface. The presence of plenty of surface species on electrodeA" cycled with pyrazole, in contrast to the bare electrode, emphasizes the key role of the pyrazole additive in the surface film formation.

The FTIR spectrum of electrode B is almost the same as that of electrode A. However, the spectrum of the electrode C revealed no new bands from organic species, which suggests that the NMC-active material plays a critical role in the electrolyte oxidation and formation of the surface film.

The IR signature of the pyrazole additive was not detectable, even though the CV measurements clearly indicated that the electrochemical oxidative decomposition of pyrazole contributed to the surface film formation during the initial cycles, probably due to the low concentration level (3 wt %) of the pyrazole additive or the IR signature being hindered by the intense peaks of the base electrolyte.

Conclusions

The *ex situ* DSC and FTIR data indicate that regardless of the presence of a carbon additive, the active material NMC is mainly responsible for the oxidation and decomposition of the additive, EC/DEC, EC/DEC-derived species, and $LiPF_6$-derived compounds. This property emphasizes the key role of the active material NMC in the decomposition of the electrolyte and the formation of the surface film. This oxidative decomposition of the electrolyte was significantly enhanced when carbon black was present and thicker surface films were produced. A conductive carbon additive appeared to provide and maintain electron conductivity within the composite cathode and facilitated the surface film formation.

Acknowledgments. This work was supported by the National Research Foundation of Korea Grant funded by the Korean Government (MEST) (NRF-2009-C1AAA001-2009-0093307).

References

1. Xiao, L.; Ai, X.; Cao, Y.; Yang, Y. *Electrochim. Acta* **2004**, *49*, 4189.
2. Abe, T.; Takaya, T.; Yoshitake, H.; Ushigoe, Y.; Yoshio, M.; Wang, H. *Electrochem. Solid-State Lett.* **2004**, *7*, A462.
3. Cho, Y. H.; Kim, K.; Ahn, S.; Liu, H. K. *J. Power Sources* **2011**, *196*, 1483.
4. Zhang, H. P.; Xia, Q.; Wang, B.; Yang, L. C.; Wu, Y. P.; Sun, D. L.; Gan, C. L.; Luo, H. J.; Bebeda, A. W.; van Ree, T. *Electrochem. Commun.* **2009**, *11*, 526.
5. Kim, K.; Ahn, S.; Kim, H. S.; Liu, H. K. *Electrochim. Acta* **2009**, *54*, 2259.
6. Song, S.-W.; Zhuang, G. V.; Ross, P. N. *J. Electrochem. Soc.* **2004**, *151*, A1162.
7. Aurbach, D. *J. Power Sources* **2000**, *89*, 206.
8. Meyer, B. M.; Leifer, N.; Sakamoto, S.; Greenbaum, S. G.; Grey, C. P. *Electrochem. Solid-State Lett.* **2005**, *8*, A145.
9. Komaba, S.; Itabashi, T.; Ohtsuka, T.; Groult, H.; Kumagai, N.; Kaplan, B.; Yashiro, H. *J. Electrochem. Soc.* **2005**, *152*.
10. Kam, D.; Kim, K.; Kim, H.-S.; Liu, H. K. *Electrochem. Commun.* **2009**, *11*, 1657.
11. Kerlau, M.; Kostecki, R. *J. Electrochem. Soc.* **2006**, *153*, A1644.
12. Peres, J. P.; Perton, F.; Audry, C.; Biensan, P.; de Guibert, A.; Blanc, G.; Broussely, M. *J. Power Sources* **2001**, *97-98*, 702.
13. Baba, Y.; Okada, S.; Yamaki, J.-I. *Solid State Ionics* **2002**, *148*, 311.
14. Nazri, G.-A.; Pistoia, G. *Lithium Batteries: Science and Technology*; Chapter 17, Kluwer Academic Publications: 2004.
15. Julien, C. *Solid State Ionics* **2000**, *136-137*, 887.
16. Matsumoto, K.; Kuzuo, R.; Takeya, K.; Yamanaka, A. *J. Power Sources* **1999**, *81*, 558.
17. Noh, M.; Lee, Y.; Cho, J. *J. Electrochem. Soc.* **2006**, *153*, A935.
18. Zhuang, G. V.; Ross, P. N. *Electrochem. Solid-State Lett.* **2003**, *6*, A136.
19. Colthup, N. B.; Daly, L. H.; Wiberley, S. E. *Introduction to Infrared and Raman Spectroscopy*, 3rd ed.; Academic Press: New

York, 1990.
20. Socrates, G. *Infrared Characteristic Group Frequencies, Tables and Charts*, 2nd ed.; John Wiley & Sons: New York, 1994.
21. Kanamura, K.; Umegaki, T.; Ohashi, M.; Toriyama, S.; Shiraishi, S.; Takehara, Z. *Electrochim. Acta* **2001**, *47*, 433.
22. Yabuuchi, N.; Makimura, Y.; Ohzuku, T. *J. Electrochem. Soc.* **2007**, *154*, A314.
23. Yoon, W.-S.; Chung, K. Y.; McBreen, J.; Yang, X.-Q. *Electrochem. Commun.* **2006**, *8*, 1257.
24. Daasch, L. W.; Smith, D. C. *Anal. Chem.* **1951**, *23*, 853.
25. Lu, Y.-C.; Mansour, A. N.; Yabuuchi, N. Yang, S. H. *Chem. Mater.* **2009**, *21*, 4408.
26. Balasubramanian, M.; Lee, H. S.; Sun, X.; Yang, X. Q.; Moodenbaugh, A. R.; McBreen, J.; Fischer, D. A.; Fu, Z. *Electrochem. Solid-State Lett.* **2002**, *5*, A22.